


Article

Electro-Assisted Fe³⁺/Persulfate System for the Degradation of Bezafibrate in Water: Kinetics, Degradation Mechanism, and Toxicity

Yuqiong Gao , Kexuan Li, Xiangmei Zhong and Han Ning

School of Environment and Architecture, University of Shanghai for Science and Technology, Shanghai 200093, China; 18109198060@163.com (K.L.); zxm_sherry@163.com (X.Z.); nihangogo@163.com (H.N.)

* Correspondence: gaoyq@usst.edu.cn

Abstract: In this study, an electrochemical-assisted ferric ion/persulfate (EC/Fe³⁺/PS) process was proposed to degrade bezafibrate (BZF), a widespread hypolipidemic drug, in water. By promoting the reduction of Fe³⁺ to Fe²⁺ at the cathode, the introduction of an electric field successfully overcomes the limitation of non-regenerable Fe²⁺ inherent in Fe²⁺/PS systems, significantly improving the degradation efficiency of BZF. The predominant reactive species identified were •OH and SO₄^{•-}, with ¹O₂ also playing a role. Various key operational parameters were investigated and optimized, including the current intensity, Fe³⁺ dosage, PS concentration, and initial pH. With a current intensity of 50 mA, an Fe³⁺ concentration of 50 μM, a PS dosage of 50 μM, and an initial pH of 3, the degradation efficiency of BZF demonstrated an exceptional achievement, reaching up to 98.8% within 30 min. The influence of anions and humic acid was also assessed. An LC/TOF/MS analysis revealed four major degradation pathways of BZF: hydroxylation, amino bond cleavage, dechlorination, and fibrate chain removal. The acute and chronic toxicities of BZF and its degradation intermediates were then assessed using the ECOSAR program. These findings highlight the wide-ranging applications of the EC/Fe³⁺/PS system and its potential for remediating water contaminated with micropollutants.

Keywords: bezafibrate; electrochemistry; Fe³⁺/persulfate; reaction mechanism; toxicity evaluation



Citation: Gao, Y.; Li, K.; Zhong, X.; Ning, H. Electro-Assisted Fe³⁺/Persulfate System for the Degradation of Bezafibrate in Water: Kinetics, Degradation Mechanism, and Toxicity. *Water* **2024**, *16*, 649. <https://doi.org/10.3390/w16050649>

Academic Editor: Stefanos Giannakis

Received: 1 February 2024

Revised: 15 February 2024

Accepted: 21 February 2024

Published: 22 February 2024



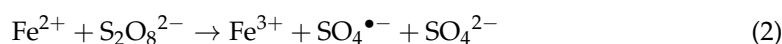
Copyright: © 2024 by the authors. Licensee MDPI, Basel, Switzerland. This article is an open access article distributed under the terms and conditions of the Creative Commons Attribution (CC BY) license (<https://creativecommons.org/licenses/by/4.0/>).

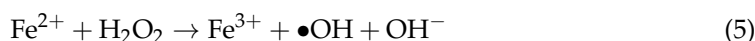
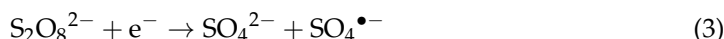
1. Introduction

Since the 1970s, traces of pharmaceuticals and personal care products (PPCPs) have been detected in various water systems [1]. These substances are of increasing concern due to their potential adverse health and ecological effects on aquatic ecosystems [2]. The concentration levels of PPCPs in natural water range from ng/L to μg/L [3]. Their persistence, resistance to degradation, and potential for bioaccumulation raise concerns about the safety of aquatic and terrestrial life [1]. Among these PPCPs, fibrate pharmaceuticals are widely prescribed for lipid regulation, especially in developed countries, with an estimated annual consumption of hundreds of tons [4]. Bezafibrate (BZF) is one of the most commonly used fibrate pharmaceuticals [5] and is frequently detected in both wastewater treatment plants and natural water bodies. For instance, BZF concentrations as high as 62.8 ng/L have been reported at a wastewater treatment plant (WWTP) in Beijing, China [6]. Additionally, BZF concentrations of 78.4 ng/L and 27 ng/L have been detected in drinking water treatment plants in Spain and Germany, respectively [7,8]. BZF has been identified as a potential endocrine disruptor [5]. Chronic exposure to certain concentrations of BZF can potentially cause myotoxic effects in specific human cell lines, endocrine disruption in male zebrafish, and the suppression of bioluminescence activity in *Aliivibrio fischeri*, among other detrimental impacts [9]. Conventional water treatment techniques often fail to completely eliminate PPCPs, including BZF, from wastewater. Thus, it is crucial to explore more efficient strategies to address the presence of these contaminants in water.

Reactive oxygen species (ROS)-mediated advanced oxidation processes (AOPs) have demonstrated substantial efficacy in addressing the issue of PPCP contamination in water bodies through the generation and utilization of ROS entities, including the hydroxyl radical ($\bullet\text{OH}$), sulfate radical ($\text{SO}_4^{\bullet-}$), singlet oxygen ($^1\text{O}_2$), etc. $\text{SO}_4^{\bullet-}$ -based AOPs have garnered considerable interest for the remediation of contaminated water. Compared to $\bullet\text{OH}$, $\text{SO}_4^{\bullet-}$ possesses a higher redox potential (2.5–3.1 V) and a longer lifespan (30–40 μs). Furthermore, $\text{SO}_4^{\bullet-}$ displays selective reactions and demonstrates heightened responsiveness towards certain functional groups, including anilinic, carboxylic, and phenolic groups [10]. Sodium persulfate ($\text{Na}_2\text{S}_2\text{O}_8$, PS) is commonly used as a source of $\text{SO}_4^{\bullet-}$, benefiting from its features, including its economical price, high stability, and the generation of less harmful byproducts [11]. PS typically requires activation to produce $\text{SO}_4^{\bullet-}$, and there are various known activation methods, including heat, ultraviolet (UV) irradiation, high pH, transition metals, electrochemical processes, and ultrasound [12]. Among these methods, the utilization of ferrous ions (Fe^{2+}) as a PS activator has become prominent due to its cost-effectiveness, high reactivity, and environmentally friendly characteristics [13]. In a study carried out by Wang et al., the degradation of acetaminophen (ACT) in the Fe^{2+} /PS process was investigated, and it was found that the optimal molar ratio of Fe^{2+} to PS for ACT removal was 5:4 [14]. Under these optimal conditions, the Fe^{2+} /PS system demonstrated a removal efficiency of over 70% for ACT within 30 min. Li et al. conducted research examining the degradation of 2,4-dinitrotoluene via the Fe^{2+} /PS process [15]. The results showed that the degradation process unfolded in two clearly delineated stages: an initial rapid reaction, followed by a slower one. Moreover, it was found that a PS-to- Fe^{2+} molar ratio below five favored the degradation of 2,4-dinitrotoluene.

However, the activation of PS by Fe^{2+} has certain intrinsic shortcomings. On one hand, an inadequate amount of Fe^{2+} can lead to a suboptimal activation of PS, thereby diminishing the removal efficiency of the target contaminants. On the other hand, an excessive amount of Fe^{2+} ultimately transforms into a large amount of Fe^{3+} . This excess Fe^{3+} tends to precipitate as insoluble iron hydroxides, leading to a substantial production of iron sludge [16]. Moreover, excess Fe^{2+} can also consume the available $\text{SO}_4^{\bullet-}$ and/or $\bullet\text{OH}$ in the Fe^{2+} /PS system, which are necessary for degrading target pollutants. Therefore, accelerating the Fe^{3+} / Fe^{2+} redox cycle within the reaction system presents an efficient strategy to address the aforementioned challenges associated with the Fe^{2+} /PS system [17]. In order to accelerate the conversion of Fe^{3+} to Fe^{2+} , several effective measures, such as the addition of reducing reagents, the introduction of UV light, and the application of electrochemistry techniques, have been successfully implemented. For instance, ascorbic acid has been shown to effectively enhance the recycling of Fe^{3+} to Fe^{2+} , thereby sustaining a high level of Fe^{2+} during the activation of PS [18]. The decolorization effectiveness of the dye Orange G in a Fe^{2+} -ethylene diamine disuccinic acid (EDDS)-activated PS process was significantly improved with the addition of hydroxylamine [19]. This improvement is attributed to EDDS's ability to decelerate the formation of iron sludge and, in conjunction with hydroxylamine, to expedite the transformation of Fe^{3+} to Fe^{2+} , ultimately boosting the performance of PS. Wang et al. discovered that when subjected to UV radiation, the photo-Fenton system (Fe^{3+} /EDDS/ H_2O_2 /UV or Fe^{3+} /EDDS/PS/UV) was more effective in eliminating p-hydroxyphenylacetic acid (p-HPA) than the Fenton process. This enhanced performance can be ascribed to the accelerated production of Fe^{2+} triggered by the UV irradiation [20]. However, introducing reducing agents may pose an ecological burden due to the potential toxicity of these additional reductants. In actual water matrices, especially those with high turbidity, the efficacy of photoreduction is notably diminished. Nevertheless, the application of an electric field can facilitate the efficient reduction of Fe^{3+} even in complex water matrix conditions.





Integrating electrochemical techniques with the Fe^{2+} /PS system allows for the regeneration of Fe^{2+} via a cathodic reduction reaction (Equation (1)), thereby sustaining the redox cycle between Fe^{3+} and Fe^{2+} and enabling the sustained activation of PS to produce $\text{SO}_4^{\bullet-}$ while maintaining an appropriate concentration of Fe^{2+} (Equation (2)) [21]. Additionally, EC can directly activate PS to yield $\text{SO}_4^{\bullet-}$ (Equation (3)) [22]. Moreover, H_2O_2 can be generated through the electrolysis of water at the cathode surface (Equation (4)), and then additional $\bullet\text{OH}$ can be formed according to Equation (5) [23,24]. Therefore, the goals of this study are to (1) explore the effectiveness of an electrochemical-assisted Fe^{3+} /persulfate system (EC/ Fe^{3+} /PS) for the degradation of bezafibrate in water, (2) identify the predominant reactive species in the EC/ Fe^{3+} /PS system, (3) estimate and optimize the main operational conditions affecting the degradation of BZF in the EC/ Fe^{3+} /PS process, such as the current intensity, PS concentration, Fe^{3+} dosage, and initial pH level, (4) examine the impact of various water matrix constituents like HCO_3^- , Cl^- and HA on BZF degradation performance, and (5) propose potential degradation pathways and assess the toxicity of these breakdown products by employing the ECOSAR program, with reference to the identified compounds.

2. Materials and Methods

2.1. Chemicals and Reagents

Bezafibrate (BZF, $\geq 99.0\%$), sodium persulfate ($\text{Na}_2\text{S}_2\text{O}_8$, PS), ethanol (EtOH, $\geq 99.5\%$), tert-butanol (TBA, $\geq 98.0\%$), humic acid (HA, $\geq 90.0\%$), methyl phenyl sulfoxide (PMSO, $\geq 98.0\%$), methyl phenyl sulfone (PMSO₂, $\geq 97.0\%$), isopropanol (IPA, $\geq 98.0\%$), and furfuryl alcohol (FFA, $\geq 98.0\%$) were purchased from Aladdin Chemicals (Shanghai, China). Ferric sulfate ($\text{Fe}_2(\text{SO}_4)_3$, $\geq 99.0\%$), anhydrous sodium sulfate (Na_2SO_4 , $\geq 99.0\%$), sulfuric acid (H_2SO_4 , $\geq 95.0\%$), sodium hydroxide (NaOH, $\geq 96.0\%$), sodium chloride (NaCl, $\geq 99.8\%$), sodium bicarbonate (NaHCO_3 , $\geq 99.5\%$), and 1,10-phenanthroline ($\text{C}_{12}\text{H}_8\text{N}_2$, $\geq 97.0\%$) were obtained from Sinopharm Chemical Reagent Co., Ltd. (Shanghai, China). HPLC-grade acetonitrile, supplied by Merck (Darmstadt, Germany), was used as the mobile phase. Experimental solutions were prepared using pure water generated from a Milli-Q purification system (Millipore, Milford, MA, USA).

2.2. Experimental Procedures

The degradation experiment was performed in an undivided 300 mL glass reactor (see Figure 1). A commercially available mixed metal oxide plate (Ti- IrO_2 / RuO_2 , DSA) measuring 2.0 cm in width and 4.0 cm in height was used as the anode in the electrolytic cell. A carbon felt plate of the same dimensions was employed as the cathode. The two electrode plates were vertically immersed in water, maintaining a distance of 2.5 cm between them. The required constant current was supplied by a DC power supply (Dongguan Tongmen Electronic Technology Co., Ltd., Guangdong, China). The reaction temperature was maintained at 20 ± 1 °C using a constant-temperature water flow circulating within a jacketed glass beaker. Then, 250 mL of reaction solution was initially prepared by mixing predetermined concentrations of BZF and ferric sulfate. The initial solution pH was adjusted to the desired level using H_2SO_4 or NaOH. After adding a certain amount of PS, the DC power supply was turned on to initiate the electrolysis reaction. Samples were taken at intervals of 0, 2.5, 5, 10, 15, 20, 25, and 30 min, respectively. These samples were immediately quenched with an excess of methanol and filtered through a 0.45 μm filter membrane before analysis. All experiments were replicated thrice.

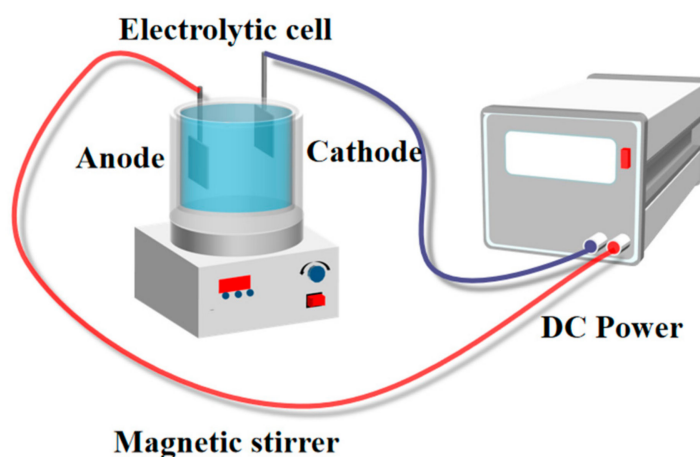


Figure 1. Scheme of the experimental equipment.

2.3. Analytical Methods

A quantitative assessment of the BZF, PMSO, and PMSO₂ concentrations was carried out via a Waters e2695 HPLC system (Waters, Milford, MA, USA), which was fitted with an UV detection unit. The detection wavelengths utilized were 235 nm for BZF, 230 nm for PMSO, and 215 nm for PMSO₂, respectively. The chromatographic column used was a Waters Symmetry C18 column (4.6 mm × 250 mm, 5 μm, Waters, Milford, MA, USA). The mobile phase for BZF comprised a blend of acetonitrile and formic acid solution (0.1%) (70:30, *v/v*), flowing at a rate of 0.80 mL/min. For PMSO and PMSO₂, the mobile phases consisted of acetonitrile and water mixtures (PMSO: 28:72, *v/v*, PMSO₂: 40:60, *v/v*) at a flow rate of 0.80 mL/min. The concentration of Fe²⁺ was measured employing the 1,10-phenanthroline colorimetric assay, utilizing a UV-vis spectrophotometer [25].

The intermediate products of BZF were analyzed using an LC/TOF/MS system, which included an Agilent 1290 UPLC unit paired with 6550 quadrupole time-of-flight mass spectrometry (Q-TOF, Agilent Technologies, Santa Clara, CA, USA). The separation was achieved on a Waters BEH C18 column (2.1 × 100 mm, 1.7 μm, Waters, Milford, MA, USA). Mobile phase A was 0.1% formic acid in pure water, while mobile phase B was acetonitrile. The elution began with a 5% B composition and lasted for 2 min. Then, it was gradually increased linearly to 95% B over a period of 15 min and maintained at 95% B for 5 min. Subsequently, the elution composition was reduced to 5% B in the next 1 min and kept at 5% B for another 7 min. The flow rate was kept constant at 0.3 mL/min. The spray voltage for ESI(+) and ESI(−) was set at 4000 V and −3200 V, respectively. The temperature for the sheath gas was regulated to 350 °C, with the flow of the sheath gas adjusted to 12 L/min.

3. Results and Discussion

3.1. Removal of BZF under Different Systems

The removal efficiency of BZF at a pH of 3.0 using various processes, namely PS alone, EC alone, Fe³⁺ alone, EC/PS, and EC/Fe³⁺/PS, was initially investigated, and the results are illustrated in Figure 2. It was evident that the use of either PS or Fe³⁺ alone was ineffective in the removal of BZF, revealing that under the tested conditions, neither PS oxidation nor ferric hydroxide flocs were capable of eliminating BZF in water. However, the removal efficiency of BZF by EC alone was more pronounced, reaching 41.9% within 30 min. This could be attributed to the direct electron transfer (DET) mechanisms occurring on the surface of the Ti/RuO₂-IrO₂ anode, coupled with the generation of •OH, according to Equation (6). Furthermore, incorporating PS into the EC process led to a notable increase in the BZF removal efficiency, reaching 63.8%, probably due to the generation of SO₄^{•−} through the electron transfer reaction described in Equation (3). Remarkably, the introduction of both PS and Fe³⁺ into the EC system facilitated a near-

complete removal of BZF, with an efficiency of 98.8% achieved within 30 min. With the EC addition, the generation of $\text{SO}_4^{\bullet-}$ was augmented not only through the direct electron transfer reaction but also via the activation of PS by Fe^{2+} , which is continuously regenerated from Fe^{3+} at the cathode [21]. Thus, a reduction cycle from Fe^{3+} to Fe^{2+} is realized in the proposed EC/ Fe^{3+} /PS system, maintaining an appropriate Fe^{2+} level that continuously activates PS to produce $\text{SO}_4^{\bullet-}$. Meanwhile, $\bullet\text{OH}$ is also generated, as explained in Equations (7) and (8) [26].

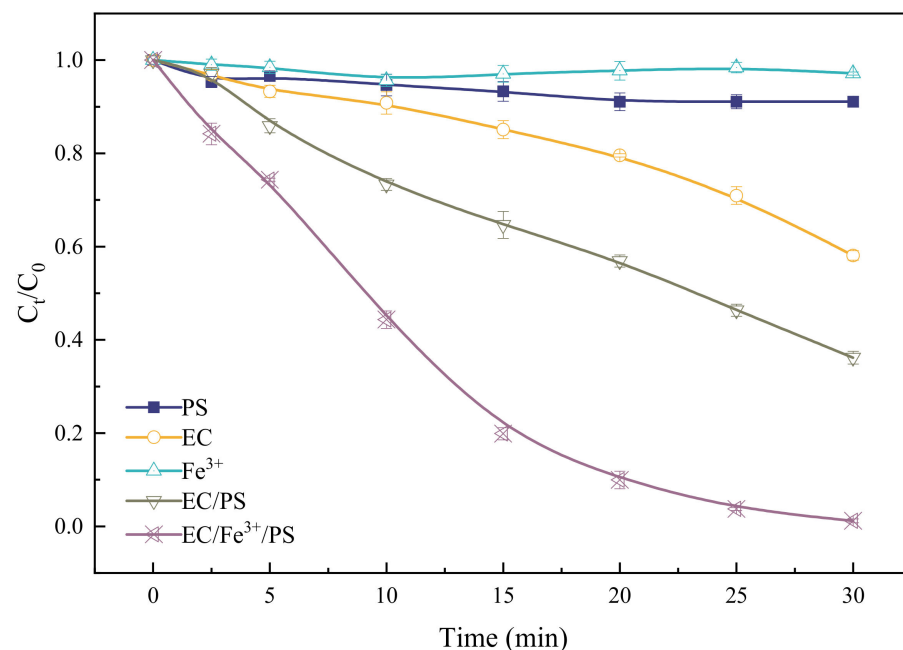
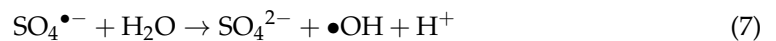


Figure 2. Removal of BZF under various processes. Conditions: $[\text{BZF}]_0 = 10 \mu\text{M}$, $[\text{Fe}^{3+}]_0 = 50 \mu\text{M}$, $[\text{PS}]_0 = 50 \mu\text{M}$, current intensity = 50 mA, $[\text{Na}_2\text{SO}_4]_0 = 25 \text{mM}$, and initial pH = 3.

Since Fe^{2+} plays a key role in the activation of PS, and the regeneration rate of Fe^{2+} is essential for maintaining excellent degradation performance in the EC/ Fe^{3+} /PS system, investigating the variation in iron species concentrations during the reaction is necessary. Figure 3 illustrates the changes in the concentrations of different valence states of iron in the solution during the reaction. The concentration of Fe^{3+} consistently decreased in the EC/ Fe^{3+} /PS process, while the concentration of Fe^{2+} gradually increased. For example, in the initial 15 min, the concentration of Fe^{2+} increased from 0 to 21.7 μM and then remained around 25 μM until the end of the reaction, indicating a relatively high conversion efficiency of Fe^{3+} to Fe^{2+} in the system. The total Fe concentration initially showed a slow decrease and then stabilized over time, which can be attributed to the deposition of some iron ions on the surface of the carbon felt (CF) cathode. The stable concentration of total Fe in the solution at the end of the reaction may be due to the adsorption saturation of CF.

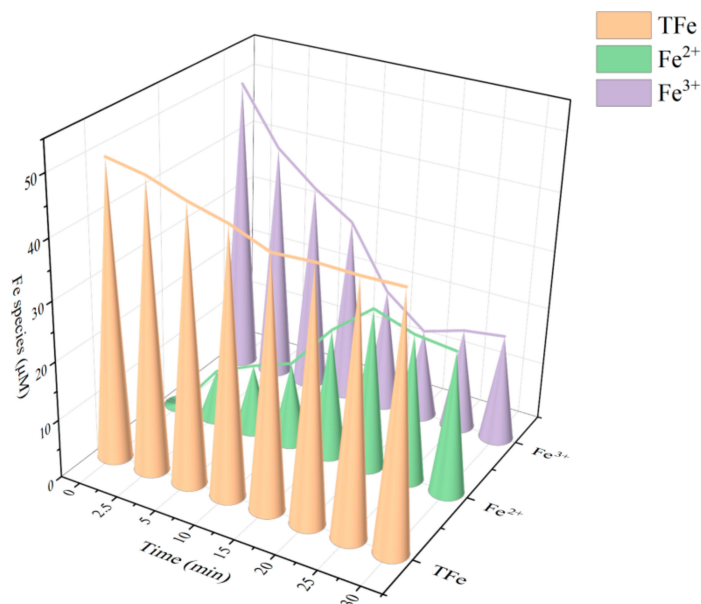


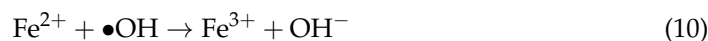
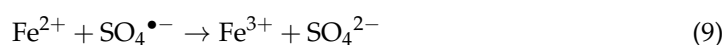
Figure 3. Changes in the concentrations of Fe^{2+} , Fe^{3+} , and total Fe during the EC/ Fe^{3+} /PS process. Conditions: $[\text{BZF}]_0 = 10 \mu\text{M}$, $[\text{Fe}^{3+}]_0 = 50 \mu\text{M}$, $[\text{PS}]_0 = 50 \mu\text{M}$, current intensity = 50 mA, $[\text{Na}_2\text{SO}_4]_0 = 25 \text{ mM}$, and initial pH = 3.

3.2. Effect of Operational Condition

3.2.1. Current Intensity

The introduction of an electric field into the Fe^{3+} /PS system can foster the sustainability of the conversion of Fe^{3+} to Fe^{2+} . Meanwhile, it can also directly induce PS to produce reactive species. Thus, the effect of different current intensities on BZF degradation in the EC/ Fe^{3+} /PS system was examined. As depicted in Figure 4a, increasing the current intensity from 10 to 50 mA led to a corresponding increase in the BZF removal efficiency, escalating from 87.8% to 98.8%. However, further increasing the current intensity led to a decrease in the removal efficiency, especially at extremely high current intensities. For example, when the current intensity reached 400 mA, the removal efficiency decreased to 36.9%. A previous study also indicated that there is an optimum current value for the electrochemical combined Fe^{3+} /PMS process [27].

The promoting effect of elevated current intensity can be attributed to three factors. Firstly, a higher current intensity accelerates the transformation of Fe^{3+} to Fe^{2+} (Equation (1)), leading to an increased activation of PS and the generation of more $\text{SO}_4^{\bullet-}$. Secondly, higher current intensities promote the reduction reaction of dissolved oxygen in water to produce H_2O_2 (Equation (4)), which can react with Fe^{2+} to form an electro-Fenton reaction and generate more $\bullet\text{OH}$ (Equation (5)). Thirdly, the direct activation of PS by EC is also expected to be enhanced under higher current intensities. However, when the current intensity was further increased from 50 to 200 and 400 mA, the degradation efficiency of BZF decreased. This phenomenon can be attributed to the generation of higher amounts of Fe^{2+} at a higher applied current. Consequently, the excess Fe^{2+} might have functioned as radical scavengers, thereby competing with BZF for $\text{SO}_4^{\bullet-}$ and $\bullet\text{OH}$ (Equations (9) and (10)) [28,29]. Additionally, higher current intensities may promote the formation of iron hydroxide precipitation, leading to the consumption of iron species [30].



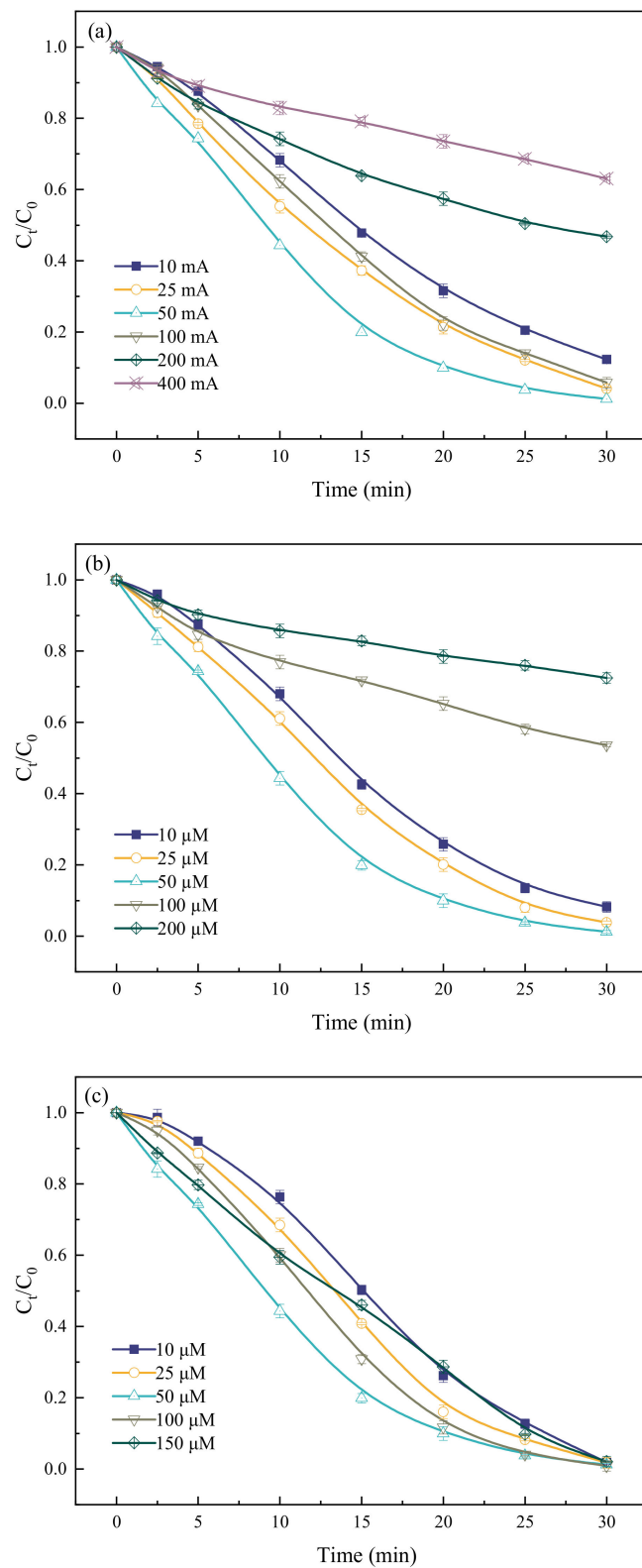


Figure 4. Cont.

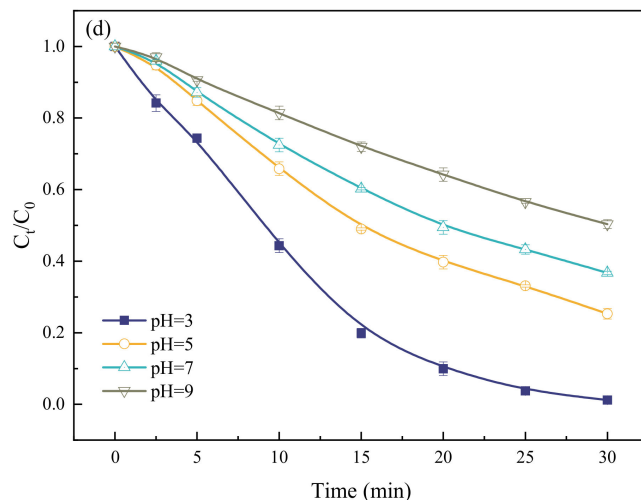


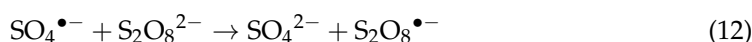
Figure 4. BZF removal under different (a) current intensities; (b) Fe^{3+} concentrations; (c) PS dosages; and (d) initial pH values in the EC/ Fe^{3+} /PS system. Conditions: $[\text{BZF}]_0 = 10 \mu\text{M}$, $[\text{Na}_2\text{SO}_4]_0 = 25 \text{ mM}$, and (a) $[\text{Fe}^{3+}]_0 = 50 \mu\text{M}$, $[\text{PS}]_0 = 50 \mu\text{M}$, current intensity = 10–400 mA, and initial pH = 3; (b) $[\text{Fe}^{3+}]_0 = 10\text{--}200 \mu\text{M}$, $[\text{PS}]_0 = 50 \mu\text{M}$, current intensity = 50 mA, and initial pH = 3; (c) $[\text{Fe}^{3+}]_0 = 50 \mu\text{M}$, $[\text{PS}]_0 = 10\text{--}150 \mu\text{M}$, current intensity = 50 mA, and initial pH = 3; and (d) $[\text{Fe}^{3+}]_0 = 50 \mu\text{M}$, $[\text{PS}]_0 = 50 \mu\text{M}$, current intensity = 50 mA, and initial pH = 3–9.

3.2.2. Fe^{3+} Concentration

The influence of varying Fe^{3+} concentrations on the degradation efficiency of BZF was also examined (Figure 4b). Elevating the Fe^{3+} concentration from 10 to 50 μM led to an enhancement in the BZF degradation efficiency, rising from 91.8% to 98.8% within 30 min. This enhancement is likely due to the augmented concentration of Fe^{2+} via cathodic reduction, which facilitates the activation of PS. Nevertheless, as the Fe^{3+} concentration further rose from 50 to 100 and 200 μM , the degradation efficiency of BZF significantly decreased from 98.8% to 46.4% and 27.5%. The decline in the BZF degradation efficiency was due to the higher Fe^{2+} concentrations resulting from the reduction of Fe^{3+} , leading to the inhibition of $\text{SO}_4^{\bullet-}$ and $\bullet\text{OH}$ accumulation because of their consumption by excess Fe^{2+} (Equations (9) and (10)) [29]. Therefore, an appropriate concentration of Fe^{3+} is important for the optimal performance of the EC/ Fe^{3+} /PS system.

3.2.3. PS Dosage

The effect of varying PS dosages on BZF degradation in the EC/ Fe^{3+} /PS process was examined, with the results displayed in Figure 4c. It was observed that there was an optimal PS dosage for achieving the highest degradation efficiency of BZF. Although the final removal efficiency was similar for different PS dosages, there was an optimal PS dosage for the initial BZF degradation rate ($\mu\text{M}/\text{min}$), which was determined by calculating the change in concentration during the initial 2.5 min and the PS dosage in the range of 10 to 150 μM . Specifically, with the increase in the PS concentration from 10 to 50 μM , the initial degradation rate of BZF rose from 0.054 $\mu\text{M}/\text{min}$ to 0.63 $\mu\text{M}/\text{min}$. However, as the PS dosage further rose to 150 μM , the initial degradation rate of BZF decreased to 0.45 $\mu\text{M}/\text{min}$. At PS dosages lower than 50 μM , more $\text{SO}_4^{\bullet-}$ was generated due to PS serving as a precursor for $\text{SO}_4^{\bullet-}$ in the EC/ Fe^{3+} /PS process. However, when the PS dosage exceeded 50 μM , excess $\text{SO}_4^{\bullet-}$ underwent self-quenching reactions or reacted with PS and $\bullet\text{OH}$, as shown in Equations (11)–(13) [14]. Consequently, there was a reduced concentration of radicals available for the degradation of BZF.





3.2.4. Initial pH

The solution pH is recognized as a pivotal factor that significantly impacts BZF degradation in the EC/Fe²⁺/PS process, as it greatly affects the form of iron species and the formation of Fe³⁺-hydroxyl complexes [31]. The degradation of BZF was investigated across an initial pH range of 3–9, with the results illustrated in Figure 4d. It was observed that the degradation efficiency of BZF monotonically decreased from 98.8% to 49.7% as the initial pH rose from 3 to 9, indicating that a lower pH was found to be more advantageous for effectively removing BZF. This is because at higher pH values above 4, Fe³⁺ ions are prone to precipitate, forming Fe(OH)₃ precipitates [19,31,32]. Meanwhile, at relatively high pH values, the soluble concentration of Fe²⁺ is also reduced, which affects the activation of PS. Furthermore, the cathodic reduction of iron ions is impeded in alkaline media, which additionally obstructs BZF degradation [33].

3.3. Identification of Reactive Species

Experiments to determine the primary reactive species in the EC/Fe³⁺/PS system were carried out through radical scavenging assays, utilizing the variance in reaction rate constants among quencher compounds and free radicals. It is commonly recognized that SO₄^{•-}, •OH, and ¹O₂ are the oxidizing species involved in PS activation. Tert-butanol (TBA) is capable of selectively scavenging •OH with a second-order rate constant of up to (3.8–8.2) × 10⁸ M⁻¹s⁻¹ [34]. In order to scavenge both SO₄^{•-} and •OH, isopropanol (IPA) was employed due to its high reactivity with both species (k_{SO₄^{•-},IPA} = (6.0–8.2) × 10⁷ M⁻¹ s⁻¹, •OH (k_{•OH,IPA} = (1.9–2.8) × 10⁹ M⁻¹ s⁻¹) [34]. Therefore, the impact of different concentrations of IPA and TBA on BZF degradation within the EC/Fe³⁺/PS system was examined, and the corresponding outcomes are depicted in Figure 5. As seen, the degradation efficiency of BZF in the EC/Fe³⁺/PS process significantly decreased from 98.8% to 49.4% and 29.3%, respectively, with the addition of 1 mM of TBA and IPA. When the scavenger concentration was further increased to 10 and 20 mM, the BZF degradation efficiency decreased to 19.1% and 6.5% with the addition of TBA and to 9.4% and 0.5% with the addition of IPA, respectively. These findings suggest that both SO₄^{•-} and •OH coexist in the EC/Fe³⁺/PS system and are the primary radicals responsible for BZF degradation, with •OH playing a more significant role than SO₄^{•-}.

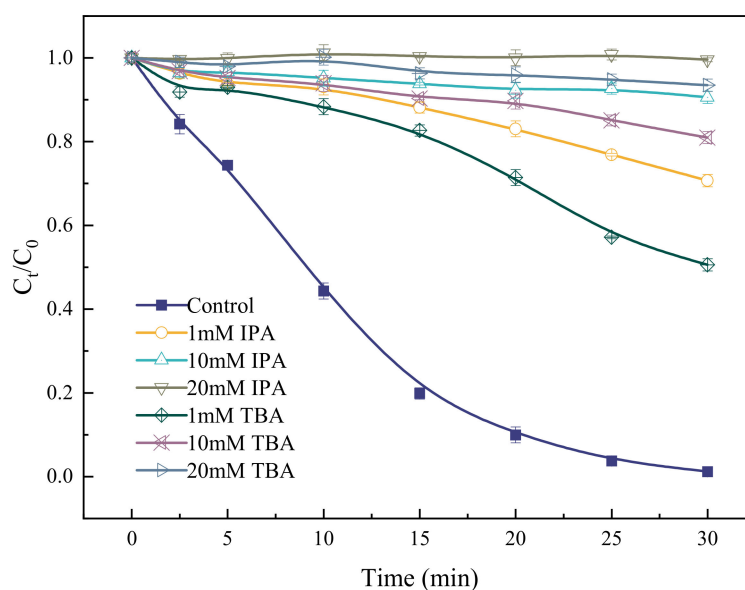


Figure 5. Effect of IPA and TBA on the degradation of BZF. Conditions: [BZF]₀ = 10 μM, [Fe³⁺]₀ = 50 μM, [PS]₀ = 50 μM, current intensity = 50 mA, [Na₂SO₄]₀ = 25 mM, and initial pH = 3.

As a non-radical oxidizing species, $^1\text{O}_2$ is commonly generated in many AOPs, including those based on PS [35]. It exhibits prominent selectivity for degrading substances and plays an important role in the removal of contaminants with electron-rich chemical bonds [36]. Furfuryl alcohol (FFA) is commonly employed as a scavenger for $^1\text{O}_2$ due to its high reaction rate constant with $^1\text{O}_2$ ($1.2 \times 10^8 \text{ M}^{-1} \text{ s}^{-1}$) [35]. Therefore, the effect of FFA on BZF degradation in the EC/ Fe^{3+} /PS process was examined, and the outcomes are depicted in Figure 6. As seen, upon introducing 0.5 mM of FFA into the system, there was a marked reduction in BZF degradation from an initial rate of 98.8% to 28.2%. With a further increase in FFA concentration, the removal of BZF was almost completely inhibited, indicating that $^1\text{O}_2$ may also play a role in BZF degradation in the EC/ Fe^{3+} /PS process. The generation of $^1\text{O}_2$ involves a two-step process. In the first step, dissolved oxygen in water can undergo direct single-electron reduction at the cathode or react with Fe^{2+} to yield $\text{O}_2^{\bullet-}$ (Equations (14) and (15)). In the second step, the $\text{O}_2^{\bullet-}$ species subsequently reacts with either H_2O or $\bullet\text{OH}$, resulting in the formation of $^1\text{O}_2$ (Equations (16) and (17)) [37].

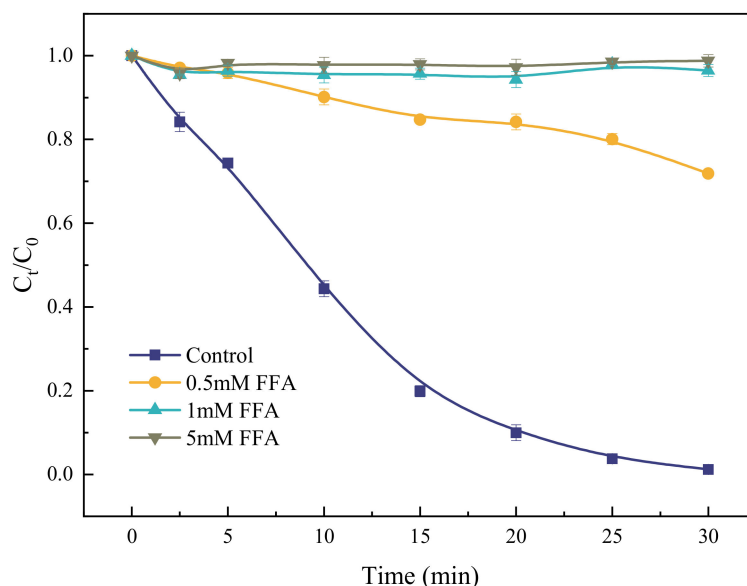
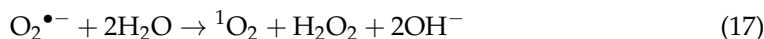
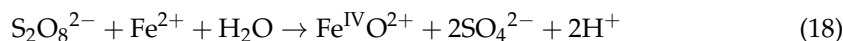


Figure 6. Effect of FFA on the degradation of BZF. Conditions: $[\text{BZF}]_0 = 10 \mu\text{M}$, $[\text{Fe}^{3+}]_0 = 50 \mu\text{M}$, $[\text{PS}]_0 = 50 \mu\text{M}$, current intensity = 50 mA, $[\text{Na}_2\text{SO}_4]_0 = 25 \text{ mM}$, and initial pH = 3.

Recently, Fe(IV) has also been recognized as a significant ROS in the Fe^{2+} /PS system (Equation (18)) [38]. Wang and colleagues [38] used PMSO as an indicator to confirm the formation of Fe(IV) species within the EC/ Fe^{3+} /PS reaction setup. Figure 7 presents the changes in the concentrations of PMSO and PMSO_2 throughout the reaction. Here, $\Delta(\text{PMSO})$ and $\Delta(\text{PMSO}_2)$ denote the respective changes in the concentrations of PMSO and PMSO_2 during the reaction. The value of $\Delta(\text{PMSO})$ continuously increased from 0 to 14.9 μM , indicating the rapid oxidation of PMSO in the system. However, the value of $\Delta(\text{PMSO}_2)$ detected within 30 min of the reaction remained below 1 μM , suggesting that the generation of Fe(IV) formed during the reaction is limited. Therefore, the contribution of Fe(IV) to BZF degradation can be considered negligible.



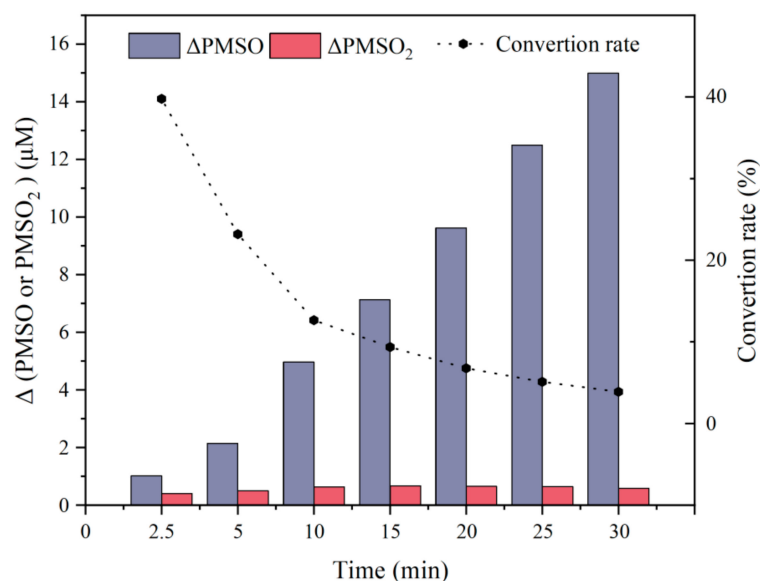


Figure 7. The variations in PMSO and PMSO₂ concentrations in the EC/Fe³⁺/PS system. Conditions: [BZF]₀ = 10 μM, [PMSO]₀ = 25 μM, [Fe³⁺]₀ = 50 μM, [PS]₀ = 50 μM, current intensity = 50 mA, [Na₂SO₄]₀ = 25 mM, and initial pH = 3.

3.4. Effect of Water Matrix

The existence of inorganic anions and natural organic matter (NOM) may influence the degradation efficiency of specific pollutants when subjected to AOPs. The extent to which these constituents enhance or inhibit the process depends on the inherent properties of the individual compounds and their interactions with the reactive radicals generated during the treatment [39]. Therefore, the effect of different water matrix components such as HCO₃[−] (0–10 mM), Cl[−] (0–10 mM), and humic acids (HA, 0–10 mg/L) on the degradation of BZF was investigated (Figure 8).

As shown in Figure 8a, when 1, 5, and 10 mM of HCO₃[−] were added, the degradation efficiency of BZF in the EC/Fe³⁺/PS system at 30 min decreased to 91.5%, 85.0%, and 77.9%, respectively, compared to the system without any additive (98.8%). This decrease can be attributed to the rapid capture of the dominant •OH and SO₄^{•−} species by HCO₃[−], leading to the formation of CO₃^{•−}, according to Equations (19) and (20). However, CO₃^{•−} has a lower oxidation capacity than •OH and SO₄^{•−}, resulting in a lower efficiency of BZF degradation [40].

The roles of Cl[−] in BZF degradation are depicted in Figure 8b, and it is important to note that Na₂SO₄ was used as a supporting electrolyte in the system. Cl[−], similar to HCO₃[−], exhibited inhibitory effects on BZF degradation, but to a slightly lesser extent. There is controversy regarding the impact of Cl[−] on the degradation of organic pollutants in electrochemical systems. Cl[−] undergoes an oxidation process at the surface of the DSA anode, which results in the formation of Cl₂ (Equation (21)). Subsequently, the Cl₂ rapidly hydrolyzes, giving rise to free chlorine species (Equation (22)), which could potentially enhance the targeted pollutant degradation [41]. However, on the other hand, the presence of Cl[−] can also have negative effects on SO₄^{•−}-based AOPs [42]. Cl[−] can react with •OH and SO₄^{•−} to generate various reactive species, including Cl•, ClOH•−, and Cl₂^{•−}, as shown in Equations (23)–(26) [42,43]. These reactive species exhibit a weaker oxidative capacity and consequently result in lower BZF degradation efficiency. Furthermore, an excessive amount of chloride can induce a more pronounced chlorine evolution, which in turn results in a reduction in the anode potential through a process named the “potentiostatic buffering phenomenon” [44]. Additionally, the formation of electrogenerated chlorate (ClO₃[−]), perchlorate (ClO₄[−]), and peroxide compounds can further impact the degradation efficiency of pollutants unfavorably [45].

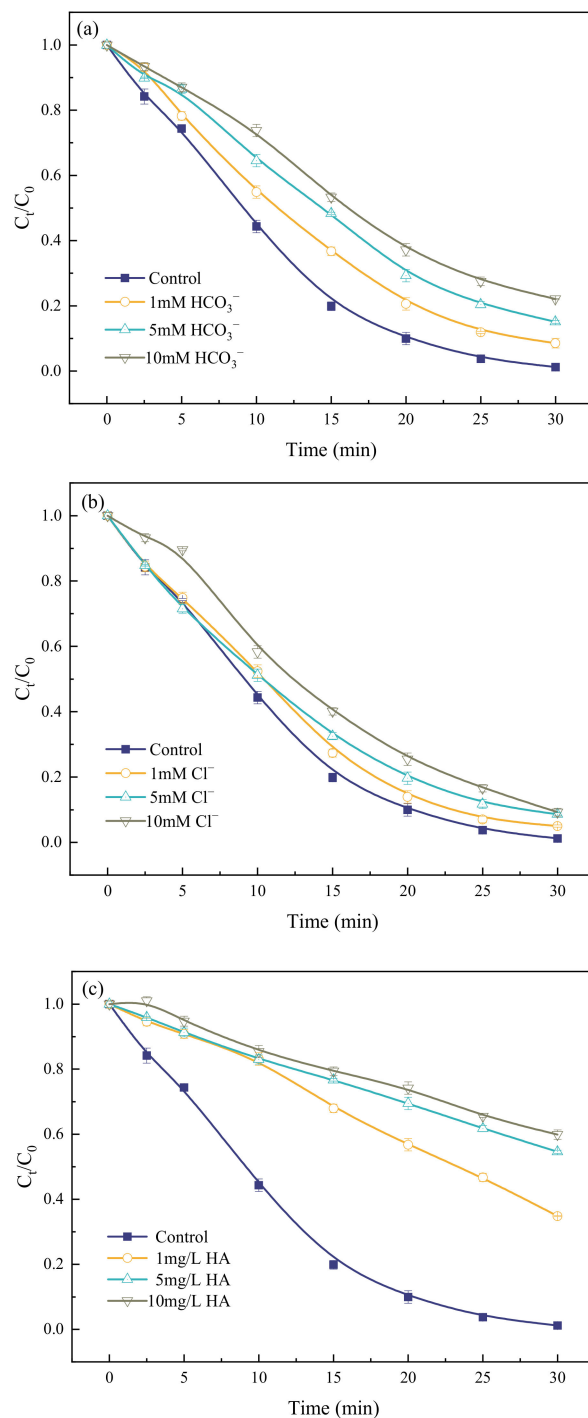
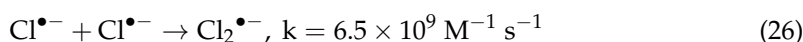
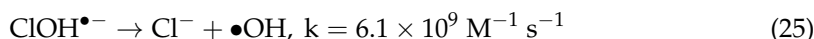
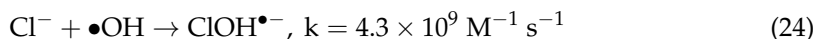
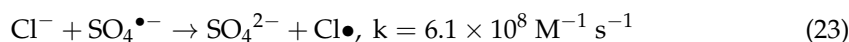
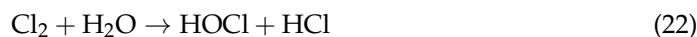
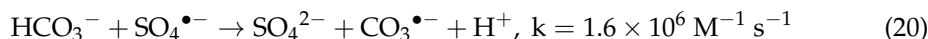
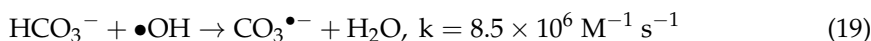


Figure 8. Effect of (a) HCO_3^- ; (b) Cl^- ; and (c) HA on the degradation of BZF in the EC/ Fe^{3+} /PS process. Conditions: $[\text{BZF}]_0 = 10 \mu\text{M}$, $[\text{Fe}^{3+}]_0 = 50 \mu\text{M}$, $[\text{PS}]_0 = 50 \mu\text{M}$, current intensity = 50 mA, $[\text{Na}_2\text{SO}_4]_0 = 25 \text{ mM}$, and initial pH = 3.

Humic acid (HA), a principal constituent of NOM and a prevalent substance in water resources, can exert a significant impact on the degradation efficacy of targeted pollutants within AOPs [46]. As shown in Figure 8c, when the HA concentration was increased from 0 to 10 mg/L, there was a remarkable decrease in the BZF degradation efficiency of the EC/ Fe^{3+} /PS process, dropping from 98.8% to 40.1%. This decrease could be due to HA competitively consuming reactive species like free radicals, thereby impeding the degradation of BZF [47].



3.5. Products Identification and Degradation Pathways

To gain deeper insight into the BZF degradation mechanism within the EC/Fe³⁺/PS system, intermediate degradation products (DPs) were identified via LC/TOF/MS. Details regarding DPs' retention times, mass-to-charge (*m/z*) ratios, and molecular structures are specified in Table 1. Additionally, the MS² spectra of BZF and its DPs are presented in Figure S1. Drawing from the identified intermediates and referencing the prior studies [5,48], the possible degradation pathways for BZF in the EC/Fe³⁺/PS system are proposed in Figure 9. Generally, BZF was degraded in the EC/Fe³⁺/PS system through four primary routes: (i) The hydroxylation of the aromatic ring structure. BZF features two aromatic rings, offering numerous potential sites for hydroxylation. Prior research indicates that the isosurface of the HOMO orbital was predominantly located on the phenoxyaromatic acid moiety of BZF, predisposing it to attack by radicals and leading to the formation of DP1. Subsequently, DP1 underwent a ring-opening reaction to yield DP2, which, upon further oxidation, resulted in the formation of DP3. (ii) The cleavage of the amino bond. The amino group (-NH-) was attacked to generate DP4 and DP5. (iii) Dechlorination. Here, BZF underwent oxidative dechlorination, resulting in the formation of DP6. (iv) Fibrate chain removal. The fibrate chain of BZF was replaced by a hydroxyl group (-OH), producing DP7. DP7 was then further oxidized to form either DP8 or DP9. These pathways highlight the multifaceted nature of BZF degradation within the EC/Fe³⁺/PS system, encompassing a range of structural modifications, from hydroxylation to the loss of functional groups.

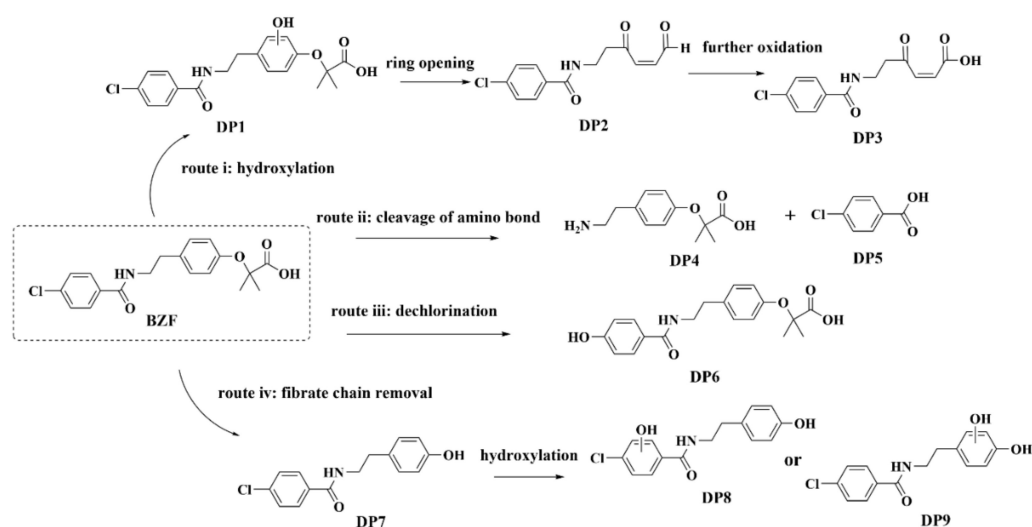


Figure 9. Possible degradation pathways for BZF.

Table 1. Summary of major degradation products of BZF identified by LC/TOF/MS.

DPs	Rt (min)	<i>m/z</i>	Molecular Formula	Structure
BZF	12.903	362.1161	C ₁₉ H ₂₀ ClNO ₄	
DP1	14.097	376.0943	C ₁₉ H ₂₀ ClNO ₅	
DP2	10.110	266.0589	C ₁₃ H ₁₂ ClNO ₃	
DP3	17.798	282.2052	C ₁₃ H ₁₂ ClNO ₄	
DP4	10.669	224.1630	C ₁₂ H ₁₇ NO ₃	
DP5	11.910	158.1545	C ₇ H ₅ ClO ₂	
DP6	6.323	344.2293	C ₁₉ H ₂₁ NO ₅	
DP7	11.227	276.0795	C ₁₅ H ₁₄ ClNO ₂	
DP8	10.048	292.0745	C ₁₅ H ₁₄ ClNO ₃	
DP9	12.717	292.0745	C ₁₅ H ₁₄ ClNO ₃	

3.6. Toxicity Evaluation

The Ecological Structure–Activity Relationship (ECOSAR) model, developed by the U.S. Environmental Protection Agency (EPA), is a useful tool for predicting the acute and chronic aquatic toxicities of pollutants to fish, daphnids, and green algae based on their chemical structure [49]. The molecular structures of BZF and its intermediate products obtained through an LC/TOF/MS analysis were inputted into the ECOSAR program (Version 2.2) and subsequently converted into predicted outcomes through theoretical computations. Figure 10 and Table S1 show the predicted acute and chronic toxicities of the degradation products of BZF, as determined by the ECOSAR program.

The acute toxicity of BZF was found to be 17.6 mg/L for fish, 12.2 mg/L for daphnids, and 4.87 mg/L for green algae. Meanwhile, the chronic toxicity values for BZF to these organisms were determined to be 0.618 mg/L for fish, 4.62 mg/L for daphnids, and 8.4 mg/L for green algae, respectively. This suggests that BZF exhibits a more pronounced chronic toxicity to fish and daphnids, whereas its acute toxicity to green algae is stronger than its chronic toxicity.

In accordance with the Globally Harmonized System of Classification and Labeling of Chemicals (GHS), organic compounds are classified into four categories based on their chronic toxicity (ChV), half-effective concentration (EC50), and half-lethal concentration

(LC50): very toxic (less than 1 mg/L), toxic (1 to 10 mg/L), harmful (10 to 100 mg/L), and not harmful (greater than 100 mg/L) [46]. Most of the detected degradation products showed a decrease in acute toxicity compared to BZF, except for DP7, which was still classified as “toxic” to all three aquatic species. In addition, despite the decrease in acute toxicity compared to their parent compounds, DP1, DP8, and DP9 were still classified as “toxic” to fish and daphnids, while DP8 and DP9 were also classified as “toxic” to green algae. In terms of chronic toxicity, most DPs also exhibited a decrease compared to BZF. However, DP7, DP8, and DP9 were more toxic than BZF to daphnids and green algae, with DP7 being classified as “very toxic”. In addition, DP1 was also classified as “toxic” to both fish and daphnid. By comparing the structures of these DPs, the control of BZF toxicity by the EC/Fe³⁺/PS process occurs through processes such as the cleavage of the amino bond, dechlorination, and ring opening. However, the hydroxylation process has the potential to increase the toxicity of DPs. A previous study has also indicated that incorporating hydroxyl groups into the precursor resulted in increased toxicity, which was attributed to the enhanced reactivity of these degradation products [50].

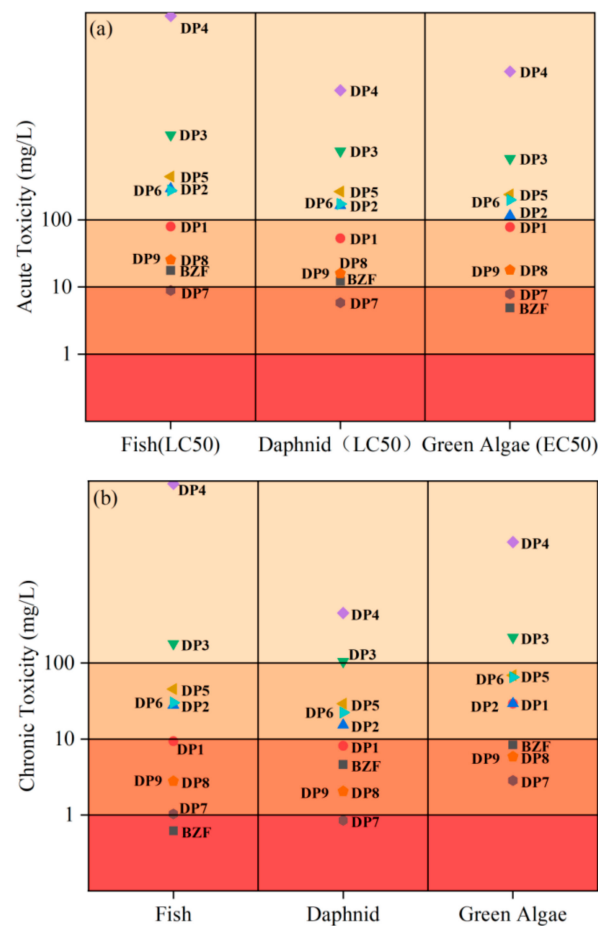


Figure 10. Toxicity assessment of BZF and its degradation products: (a) acute toxicity and (b) chronic toxicity.

4. Conclusions

This study has demonstrated that the EC/Fe³⁺/PS process is an effective approach for the elimination of micropollutants, including BZF, from aqueous solutions. Fe³⁺ could be rapidly reduced to Fe²⁺ at the cathode, which could maintain a proper Fe²⁺ level in the system that continuously activates PS to generate radicals to effectively degrade BZF. The radical scavenging tests showed that the major oxidizing species in the EC/Fe³⁺/PS system include both radicals (SO₄^{•−} and •OH) and non-radicals (¹O₂). Optimum parameters exist, including current intensity, Fe³⁺ concentration, PS dosage, and initial pH, for the removal

of BZF by the EC/Fe³⁺/PS process. Up to a 98.8% removal of BZF by the EC/Fe³⁺/PS process within 30 min can be achieved under the optimum conditions. The water matrix always exerted a negative effect on BZF degradation. Four possible BZF degradation pathways, including the hydroxylation of the aromatic ring, the cleavage of the amino bond, oxidation dechlorination, and the removal of the fibrate chain, were proposed based on the LC/TOF/MS analysis. According to toxicity predictions made using the ECOSAR software (Version 2.2), the EC/Fe³⁺/PS process generally decreased the toxicity of the BZF solution to three test aquatic species, including fish, daphnids, and green algae. This research not only deepens the understanding of the kinetics and mechanism behind BZF degradation via the EC/Fe³⁺/PS process but also highlights the potential of this approach for the removal of micropollutants from water.

Supplementary Materials: The following are available online at <https://www.mdpi.com/article/10.3390/w16050649/s1>: Figure S1: The MS² spectrum of BZF and its DPs and Table S1: Acute and chronic toxicity of BZF and its degradation products.

Author Contributions: Conceptualization, Y.G.; methodology, K.L. and X.Z.; formal analysis, Y.G. and K.L.; resources, Y.G.; data curation, K.L., X.Z. and H.N.; writing—original draft preparation, K.L. and X.Z.; writing—review and editing, Y.G., visualization, X.Z. and H.N.; supervision, Y.G., funding acquisition, Y.G. All authors have read and agreed to the published version of the manuscript.

Funding: This study was supported by the Scientific and Innovative Action Plan of Shanghai, China, (19DZ1208204) and the National Science Foundation of China (51708348).

Data Availability Statement: The raw data supporting the conclusions of this article will be made available by the authors on request.

Conflicts of Interest: The authors declare no competing interests.

References

1. Narayanan, M.; Kandasamy, S.; Lee, J. Microbial degradation and transformation of PPCPs in aquatic environment: A review. *Heliyon* **2023**, *9*, e18426. [[CrossRef](#)]
2. Samal, k.; Mahapatra, S.; Ali, M.H. Pharmaceutical Wastewater as Emerging Contaminants (EC): Treatment Technologies, Impact on Environment and Human Health. *Energy Nexus* **2022**, *6*, 100076. [[CrossRef](#)]
3. Dai, G.H.; Wang, B.; Huang, J.; Dong, R.; Deng, S.B.; Yu, G. Occurrence and source apportionment of pharmaceuticals and personal care products in the Beiyun River of Beijing, China. *Chemosphere* **2015**, *119*, 1033–1039. [[CrossRef](#)] [[PubMed](#)]
4. Lambropoulou, D.A.; Hernando, M.D.; Konstantinou, I.K.; Thurman, E.M.; Ferrer, I.; Albanis, T.A.; Alba, A.R.F. Identification of photocatalytic degradation products of bezafibrate in TiO₂ aqueous suspensions by liquid and gas chromatography. *J. Chromatogr. A* **2008**, *1183*, 38–48. [[CrossRef](#)] [[PubMed](#)]
5. Orge, C.A.; Pereira, M.F.R.; Faria, J.L. Bezafibrate removal by coupling ozonation and photocatalysis: Effect of experimental conditions. *Environ. Nanotechnol. Monit. Manag.* **2022**, *17*, 100610. [[CrossRef](#)]
6. Sui, Q.; Huang, J.; Deng, S.B.; Chen, W.W.; Yu, G. Seasonal variation in the occurrence and removal of pharmaceuticals and personal care products in different biological wastewater treatment processes. *Environ. Sci. Technol.* **2011**, *45*, 3341–3348. [[CrossRef](#)]
7. Boleda, M.R.; Galceran, M.T.; Ventura, F. Behavior of pharmaceuticals and drugs of abuse in a drinking water treatment plant (DWTP) using combined conventional and ultrafiltration and reverse osmosis (UF/RO) treatments. *Environ. Pollut.* **2011**, *159*, 1584–1591. [[CrossRef](#)]
8. Dantas, R.F.; Canterino, M.; Marotta, R.; Sans, C.; Esplugas, S.; Andreozzi, R. Bezafibrate removal by means of ozonation: Primary intermediates, kinetics, and toxicity assessment. *Water Res.* **2007**, *41*, 2525–2532. [[CrossRef](#)]
9. Kerwald, J.; Vebber, M.C.; Aguzzoli, C.; Crespo, J.D.S.; Giovanela, M. Influence of silver nanoparticle deposition on self-assembled thin films of weak polyelectrolytes/TiO₂ for bezafibrate photodegradation through central composite experimental design. *J. Environ. Chem. Eng.* **2020**, *8*, 103619. [[CrossRef](#)]
10. Cai, J.J.; Xie, J.X.; Xing, L.P.; Zhou, L.; Zhang, Q.Z.; Zhou, M.H. Enhanced mechanism of carbamazepine degradation by electrochemical activation of persulfate in flow-through system. *Sep. Purif. Technol.* **2022**, *301*, 122021. [[CrossRef](#)]
11. Liu, J.L.; Zhong, S.; Song, Y.P.; Wang, B.Q.; Zhang, F.J. Degradation of tetracycline hydrochloride by electro-activated persulfate oxidation. *J. Electroanal. Chem.* **2018**, *809*, 74–79. [[CrossRef](#)]
12. Yakamercan, E.; Aygun, A.; Simsek, H. Antibiotic ciprofloxacin removal from aqueous solutions by electrochemically activated persulfate process: Optimization, degradation pathways, and toxicology assessment. *J. Environ. Sci.* **2023**, *143*, 85–89. [[CrossRef](#)]
13. Nie, M.H.; Yan, C.X.; Xiong, X.Y.; Wen, X.M.; Yang, X.; Lv, Z.L.; Dong, W.B. Degradation of chloramphenicol using a combination system of simulated solar light, Fe²⁺ and persulfate. *Chem. Eng. J.* **2018**, *348*, 455–463. [[CrossRef](#)]

14. Wang, S.L.; Wu, J.F.; Lu, X.Q.; Xu, W.X.; Gong, Q.; Ding, J.Q.; Dan, B.S.; Xie, P.C. Removal of acetaminophen in the Fe²⁺/persulfate system: Kinetic model and degradation pathways. *Chem. Eng. J.* **2019**, *358*, 1091–1100. [[CrossRef](#)]
15. Li, X.D.; Shen, J.L.; Sun, Z.Q.; Liu, Y.Q.; Zhang, W.W.; Wu, B.; Ma, F.J.; Gu, Q.B. Degradation of 2,4-dinitrotoluene using ferrous activated persulfate: Kinetics, mechanisms, and effects of natural water matrices. *J. Environ. Chem. Eng.* **2021**, *9*, 106048. [[CrossRef](#)]
16. Rayaroth, M.P.; Oh, D.; Lee, C.S.; Kang, Y.G.; Chang, Y.S. In situ chemical oxidation of contaminated groundwater using a sulfidized nanoscale zerovalent iron–persulfate system: Insights from a box-type study. *Chemosphere* **2020**, *257*, 127117. [[CrossRef](#)] [[PubMed](#)]
17. Vicente, F.; Santos, A.; Romero, A.; Rodriguez, S. Kinetic study of diuron oxidation and mineralization by persulphate: Effects of temperature, oxidant concentration and iron dosage method. *Chem. Eng. J.* **2011**, *170*, 127–135. [[CrossRef](#)]
18. Hu, C.K.; Chen, M.J.; Wang, L.; Ding, Y.Z.; Li, Q.S.; Li, X.Y.; Deng, J. Dual promoted ciprofloxacin degradation by Fe⁰/PS system with ascorbic acid and pre-magnetization. *Chemosphere* **2023**, *336*, 139202. [[CrossRef](#)]
19. Han, D.H.; Wan, J.Q.; Ma, Y.W.; Wang, Y.; Huang, M.Z.; Chen, Y.M.; Li, D.Y.; Guan, Z.Y.; Li, Y. Enhanced decolorization of Orange G in a Fe(II)-EDDS activated persulfate process by accelerating the regeneration of ferrous iron with hydroxylamine. *Chem. Eng. J.* **2014**, *256*, 316–323. [[CrossRef](#)]
20. Wang, X.N.; Dong, W.B.; Brigante, M.; Mailhot, G. Hydroxyl and sulfate radicals activated by Fe(III)-EDDS/UV: Comparison of their degradation efficiencies and influence of critical parameters. *Appl. Catal. B* **2019**, *245*, 271–278. [[CrossRef](#)]
21. Wu, J.; Zhang, H.; Qiu, J.J. Degradation of Acid Orange 7 in aqueous solution by a novel electro/Fe²⁺/peroxydisulfate process. *J. Hazard. Mater.* **2012**, *215–216*, 138–145. [[CrossRef](#)]
22. Santos, A.J.; Fortunato, M.S.K.V.; Lanza, M.R.V. Recent advances in electrochemical water technologies for the treatment of antibiotics: A short review. *Curr. Opin. Electrochem.* **2021**, *26*, 100674. [[CrossRef](#)]
23. Kim, C.; Ahn, J.Y.; Kim, T.Y.; Hwang, I. Mechanisms of electro-assisted persulfate/ nano-Fe⁰ oxidation process: Roles of redox mediation by dissolved Fe. *J. Hazard. Mater.* **2020**, *388*, 121739. [[CrossRef](#)] [[PubMed](#)]
24. Yuan, S.H.; Liao, P.; Alshwabkeh, A.N. Electrolytic manipulation of persulfate reactivity by iron electrodes for trichloroethylene degradation in groundwater. *Environ. Sci. Technol.* **2014**, *48*, 656–663. [[CrossRef](#)] [[PubMed](#)]
25. Zeng, H.X.; Shen, S.W.; Cai, A.H.; Sun, Q.; Wang, L.; Zhu, S.J.; Li, X.Y.; Deng, J. Degradation of tetracycline by UV/Fe³⁺/persulfate process: Kinetics, mechanism, DBPs yield, toxicity evaluation and bacterial community analysis. *Chemosphere* **2022**, *307*, 136072. [[CrossRef](#)]
26. Liang, C.J.; Su, H.W. Identification of sulfate and hydroxyl radicals in thermally activated persulfate. *Ind. Eng. Chem. Res.* **2009**, *48*, 5558–5562. [[CrossRef](#)]
27. Lin, H.; Wu, J.; Zhang, H. Degradation of clofibric acid in aqueous solution by an EC/Fe³⁺/PMS process. *Chem. Eng. J.* **2014**, *224*, 514–521. [[CrossRef](#)]
28. Cai, C.; Zhang, H.; Hou, L.W. Electrochemical enhanced heterogeneous activation of peroxydisulfate by Fe-Co/SBA-15 catalyst for the degradation of Orange II in water. *Water Res.* **2014**, *66*, 473–485. [[CrossRef](#)] [[PubMed](#)]
29. Feng, Y.; Wu, D.L.; Li, H.L.; Bai, J.F.; Hu, Y.B.; Liao, C.Z.; Li, X.Y.; Shih, K. Activation of persulfates using siderite as a source of ferrous ions: Sulfate radical production, stoichiometric efficiency, and implications. *ACS Sustain. Chem. Eng.* **2018**, *6*, 3624–3631. [[CrossRef](#)]
30. Luo, Z.P.; Liu, M.T.; Tang, D.Y.; Xu, Y.; Ran, H.H.; He, J.; Chen, K.; Sun, J. High H₂O₂ selectivity and enhanced Fe²⁺ regeneration toward an effective electro-Fenton process based on a self-doped porous biochar cathode. *Appl. Catal. B* **2022**, *315*, 121523. [[CrossRef](#)]
31. Cai, A.H.; Ling, X.; Wang, L.; Sun, Q.; Zhou, S.Q.; Chu, W.H.; Li, X.Y.; Deng, J. Insight into UV-LED/PS/Fe(III) and UV-LED/PMS/Fe(III) for p-arsanilic acid degradation and simultaneous arsenate immobilization. *Water Res.* **2022**, *223*, 118989. [[CrossRef](#)]
32. Rao, Y.F.; Vue, D.; Pan, H.M.; Feng, J.T.; Li, Y.J. Degradation of ibuprofen by a synergistic UV/Fe(III)/Oxone process. *Chem. Eng. J.* **2016**, *283*, 65–75. [[CrossRef](#)]
33. Lakshmanan, D.; Clifford, D.A.; Samanta, G. Ferrous and ferric ion generation during iron electrocoagulation. *Environ. Sci. Technol.* **2009**, *43*, 3853–3859. [[CrossRef](#)]
34. Xiong, L.L.; Ren, W.; Lin, H.; Zhang, H. Efficient removal of bisphenol A with activation of peroxydisulfate via electrochemically assisted Fe(III)-nitrioltriacetic acid system under neutral condition. *J. Hazard. Mater.* **2021**, *403*, 123874. [[CrossRef](#)]
35. Zhu, S.S.; Li, X.J.; Kang, J.; Duan, X.G.; Wang, S.B. Persulfate Activation on Crystallographic Manganese Oxides: Mechanism of Singlet Oxygen Evolution for Nonradical Selective Degradation of Aqueous Contaminants. *Environ. Sci. Technol.* **2019**, *53*, 307–315. [[CrossRef](#)] [[PubMed](#)]
36. Zhao, H.Q.; Song, J.S.; Lu, P.L.; Mu, Y. Single atom Co-anchored nitrogen-doped graphene for peroxydisulfate activation with high selectivity of singlet oxygen generation. *Chem. Eng. J.* **2023**, *456*, 141045. [[CrossRef](#)]
37. Li, J.Y.; Xiong, Z.K.; Yu, Y.H.; Wang, X.H.; Zhou, H.Y.; Huang, B.K.; Wu, Z.L.; Yu, C.X.; Chen, T.T.; Pan, Z.C.; et al. Efficient degradation of carbamazepine by electro-Fenton system without any extra oxidant in the presence of molybdate: The role of slow release of iron ions. *Appl. Catal. B* **2021**, *298*, 120506. [[CrossRef](#)]
38. Wang, Z.; Jiang, J.; Pang, S.Y.; Zhou, Y.; Guan, C.T.; Gao, Y.; Li, J.; Yang, Y.; Qiu, W.; Jiang, C.C. Is sulfate radical really generated from peroxydisulfate activated by iron(II) for environmental decontamination? *Environ. Sci. Technol.* **2018**, *52*, 11276–11284. [[CrossRef](#)] [[PubMed](#)]

39. Philip, J.M.; Koshy, C.M.; Aravind, U.K.; Aravindakumar, C.T. Sonochemical degradation of DEET in aqueous medium: Complex by-products from synergistic effect of sono-Fenton-New insights from a HRMS study. *J. Environ. Chem. Eng.* **2022**, *10*, 107509. [[CrossRef](#)]
40. Ghauch, A.; Baalbaki, A.; Amasha, M.; Asmar, R.E.; Tantawi, O. Contribution of persulfate in UV-254 nm activated systems for complete degradation of chloramphenicol antibiotic in water. *Chem. Eng. J.* **2017**, *317*, 1012–1025. [[CrossRef](#)]
41. Zhang, Y.Q.; Wang, H.J.; Li, Y.; Wang, B.; Huang, J.; Deng, S.B.; Yu, G.; Wang, Y.J. Removal of micropollutants by an electrochemically driven UV/chlorine process for decentralized water treatment. *Water Res.* **2020**, *183*, 116115. [[CrossRef](#)]
42. Lai, W.W.P.; Lin, J.C.; Li, M.H. Degradation of benzothiazole by the UV/persulfate process: Degradation kinetics, mechanism and toxicity. *J. Photochem. Photobiol. A.* **2023**, *436*, 114355. [[CrossRef](#)]
43. Pan, M.W.; Wu, Z.H.; Tang, C.Y.; Guo, K.H.; Cao, Y.J.; Fang, J.Y. Emerging investigators series: Comparative study of naproxen degradation by the UV/chlorine and the UV/H₂O₂ advanced oxidation processes. *Environ. Sci. Water Res. Technol.* **2018**, *4*, 1219. [[CrossRef](#)]
44. Elhadi, H.L.; Frontistis, Z.; Amar, H.A.; Amrani, S.; Mantzavinos, D. Electrochemical oxidation of pesticide thiamethoxam on boron doped diamond anode: Role of operating parameters and matrix effect. *Process Saf. Environ. Prot.* **2018**, *116*, 535–541. [[CrossRef](#)]
45. Zhang, C.Y.; Du, X.M.; Zhang, Z.F.; Fu, D.G. The peculiar roles of chloride electrolytes in BDD anode cells. *RSC Adv.* **2016**, *6*, 65638–65643. [[CrossRef](#)]
46. Xu, M.Y.; Deng, J.; Cai, A.H.; Ye, C.; Ma, X.Y.; Li, Q.S.; Zhou, S.Q.; Li, X.Y. Synergistic effects of UVC and oxidants (PS vs. Chlorine) on carbamazepine attenuation: Mechanism, pathways, DBPs yield and toxicity assessment. *Chem. Eng. J.* **2021**, *413*, 127533. [[CrossRef](#)]
47. Sun, Q.Y.; Wu, S.B.; Yin, R.; Bai, X.J.; Bhunia, A.K.; Liu, C.Q.; Zheng, Y.Y.; Wang, F.F.; Blatchley III, R.E. Effects of fulvic acid size on microcystin-LR photodegradation and detoxification in the chlorine/UV process. *Water Res.* **2021**, *193*, 116893. [[CrossRef](#)] [[PubMed](#)]
48. Wu, Y.X.; Yang, Y.; Liu, Y.Z.; Zhang, L.Q.; Feng, L. Modelling study on the effects of chloride on the degradation of bezafibrate and carbamazepine in sulfate radical-based advanced oxidation processes: Conversion of reactive radicals. *Chem. Eng. J.* **2019**, *358*, 1332–1341. [[CrossRef](#)]
49. Sanderson, H.; Johnson, D.J.; Wilson, C.J.; Brain, R.A.; Solomom, K.R. Probabilistic hazard assessment of environmentally occurring pharmaceuticals toxicity to fish, daphnids and algae by ECOSAR screening. *Toxicol. Lett.* **2003**, *144*, 383–395. [[CrossRef](#)] [[PubMed](#)]
50. Pang, W.C.; Yao, J.; Knudsen, T.S.; Cao, Y.; Liu, B.; Li, H.; Li, M.M.; Zhu, J.J. Degradation of three typical hydroxamic acids collectors via UVA-B activated H₂O₂ and persulfate: Kinetics, transformation pathway, DFT calculation and toxicity evaluation. *Chem. Eng. J.* **2023**, *451*, 138–639. [[CrossRef](#)]

Disclaimer/Publisher’s Note: The statements, opinions and data contained in all publications are solely those of the individual author(s) and contributor(s) and not of MDPI and/or the editor(s). MDPI and/or the editor(s) disclaim responsibility for any injury to people or property resulting from any ideas, methods, instructions or products referred to in the content.